

# Discovery of a Novel Sn(II)-Based Oxide $\beta$ -SnMoO<sub>4</sub> for Daylight-Driven Photocatalysis

Hiroyuki Hayashi,\* Shota Katayama, Takahiro Komura, Yoyo Hinuma, Tomoyasu Yokoyama, Ko Mibu, Fumiyasu Oba, and Isao Tanaka\*

Daylight-driven photocatalysts have attracted much attention in the context of “green” technology. Although various active materials have been reported and their applications are rapidly increasing, many are discovered after enormous experimental efforts. Herein the discovery of a novel oxide photocatalyst,  $\beta$ -SnMoO<sub>4</sub>, is demonstrated via a rational search of 3483 known and hypothetical compounds with various compositions and structures over the whole range of SnO-MO<sub>q/2</sub> (M: Ti, Zr, and Hf ( $q = 4$ ); V, Nb, and Ta ( $q = 5$ ); Cr, Mo, and W ( $q = 6$ )) pseudobinary systems. Screening using thermodynamic stability, band gap, and band-edge positions by density functional theory calculations identifies  $\beta$ -SnMoO<sub>4</sub> as a potential target. Then a low temperature route is used to successfully synthesize the novel crystal, which is confirmed by X-ray powder diffraction and Mössbauer spectroscopy.  $\beta$ -SnMoO<sub>4</sub> is active for the photocatalytic decomposition of a methylene blue solution under daylight and its activity is comparable to a known photocatalyst,  $\beta$ -SnWO<sub>4</sub>.

## 1. Introduction

Extensive research has been devoted to exploring new candidate materials for daylight-driven photocatalysts.<sup>[1–4]</sup> Photocatalysis occurs on the catalytic surface via a combination of complicated reaction pathways, making quantitative predictions of the performance difficult even with leading edge ab initio calculations. However, the photocatalytic activity can be qualitatively understood by the efficiency of forming electron–hole pairs because the creation of electron–hole pairs generally initiates photocatalysis.

The energies of the valence/conduction band edges with respect to photocatalytic reactions (such as water oxidation and reduction) can be used to elucidate the photocatalytic activity. In nontransition

metal oxides, the valence band maximum (VBM) is typically composed of the O-2p states, whereas the conduction band minimum (CBM) is composed of the cation states. The VBM is often modified by choosing  $ns^2$  elements as cations, such as Sn(II) and Bi(III). SnO is one example that shows p-type conductivity.<sup>[5–7]</sup>

A few oxides of  $ns^2$  elements exhibit high daylight photocatalytic activities, including BiVO<sub>4</sub>,<sup>[8–12]</sup> Bi<sub>2</sub>WO<sub>6</sub>,<sup>[13–15]</sup> and CaBi<sub>2</sub>O<sub>4</sub><sup>[16]</sup> with Bi(III); and Sn<sub>3</sub>O<sub>4</sub>,<sup>[17]</sup> SnNb<sub>2</sub>O<sub>6</sub>,<sup>[18,19]</sup> Sn<sub>2</sub>Nb<sub>2</sub>O<sub>7</sub>,<sup>[18,20]</sup> Sn<sub>2</sub>Ta<sub>2</sub>O<sub>7</sub>,<sup>[18,20]</sup> and SnWO<sub>4</sub><sup>[21,22]</sup> with Sn(II). Among them,  $\beta$ -SnWO<sub>4</sub> has been reported to show a superior photocatalytic activity for organic contaminant degradation under simulated daylight compared to BiVO<sub>4</sub>,<sup>[22]</sup> which is a promising photocatalyst. The present study aims to explore novel daylight-driven photocatalysts within Sn(II)-based complex oxides. The Inorganic Crystal Structure Database (ICSD)<sup>[23]</sup> contains  $\approx 60$  ternary Sn(II) oxides, but some are duplicate listings and polymorphs. Figure S1 (Supporting Information) shows cation elements with integral valences included in these Sn(II) ternary oxides. These cations can be categorized into three classes: 1A (alkali metal), 4A–6A, and 3B–6B groups. Oxides with alkali metals are unsuited for photocatalysts due to their poor stability in water, whereas oxides with 3B–6B group elements, which are typically comprised of robust oxyanions such as BO<sub>3</sub><sup>3-</sup>, CO<sub>3</sub><sup>2-</sup>, SO<sub>4</sub><sup>2-</sup>, and PO<sub>4</sub><sup>3-</sup>, tend to show rather wide band gaps. Hence, our research focuses on ternary Sn(II) oxides with  $qA$  group elements ( $q = 4, 5, \text{ and } 6$ ) of  $nd^0$  states, SnO-MO<sub>q/2</sub>, which have

Dr. H. Hayashi, Dr. S. Katayama, T. Komura,  
Dr. Y. Hinuma, T. Yokoyama, Prof. F. Oba,  
Prof. I. Tanaka  
Department of Materials Science and Engineering  
Kyoto University  
Sakyo, Kyoto 606-8501, Japan  
E-mail: hayashi.hiroyuki.5w@gmail.com;  
tanaka@cms.mtl.kyoto-u.ac.jp

Dr. H. Hayashi, Dr. Y. Hinuma, Prof. F. Oba,  
Prof. I. Tanaka  
Center for Materials Research by Information Integration  
National Institute for Materials Science  
Tsukuba 305-0047, Japan

Prof. K. Mibu  
Graduate School of Engineering  
Nagoya Institute of Technology  
Showa-ku, Nagoya, Aichi 466-8555, Japan

Prof. F. Oba  
Materials and Structures Laboratory  
Tokyo Institute of Technology  
Yokohama 226-8503, Japan

Prof. I. Tanaka  
Nanostructures Research Laboratory  
Japan Fine Ceramics Center  
Nagoya 456-8587, Japan

This is an open access article under the terms of the Creative Commons Attribution License, which permits use, distribution and reproduction in any medium, provided the original work is properly cited.

DOI: 10.1002/adv.201600246



a valency of  $+q$ . The empty d-band formally contributes to the CBM but not to the VBM.

## 2. Results

### 2.1. Screening via Density Functional Theory (DFT) Calculations

Although the ICSD contains only eight compounds within SnO-MO<sub>q/2</sub> pseudobinary systems, we carried out DFT calculations for 3483 SnO-MO<sub>q/2</sub> pseudobinary compounds, most of which are hypothetical compounds listed in neither the ICSD nor theoretical databases such as Materials Project Database<sup>[24]</sup> and affolib,<sup>[25]</sup> but their prototype structures and some chemical compositions are registered in the ICSD as ternary compounds. For example, when the AB<sub>2</sub>X<sub>4</sub>-type structure is listed in the ICSD as a structure prototype, we performed DFT calculations for Sn<sub>2</sub>MO<sub>4</sub> ( $M = \text{Ti, Zr, and Hf}$ ) with the AB<sub>2</sub>X<sub>4</sub>-type structure. There are 584 for  $q = 4$ , 201 for  $q = 5$ , and 362 for  $q = 6$  registered prototype structures in the ICSD. In addition, 2, 6, and 6 additional structures were examined for  $q = 4$ ,  $q = 5$ , and  $q = 6$  systems, respectively. Although their prototype structures are not registered, Sn(II) ternary oxides with these structures, such as Sn<sub>2</sub>SO<sub>5</sub>, are registered in the ICSD.

Figure 1a shows the formation energies from the DFT calculations relative to the end-members (i.e., SnO and MO<sub>q/2</sub>) with the lowest energy structures as well as the convex hull of the formation energy. Among the 3483 ternary compounds, 28 are located either on the convex hull or within 5 meV per atom above the convex hull. Separate calculations using density functional perturbation theory (DFPT) indicate that only one of these compounds has imaginary phonon modes at the  $\Gamma$  point, implying that the other 27 compounds are dynamically stable for the  $\Gamma$  point phonon mode. Hereafter, these 27 compounds are called thermodynamically stable ternary compounds.

Table S1 (Supporting Information) shows detailed information about these compounds. Of the SnO-MO<sub>q/2</sub> pseudobinary systems, eight are listed in the ICSD (Table S2, Supporting Information). Of these, six are thermodynamically stable. The exceptions are Sn<sub>2</sub>Ta<sub>2</sub>O<sub>7</sub>, which has the pyrochlore structure, and Sn<sub>3</sub>WO<sub>6</sub> because they do not meet the present definition of thermodynamically stable compounds. However, these two compounds may be stabilized at a finite temperature (e.g., due to the phonon effect). The remaining 21 thermodynamically stable ternary compounds are not included in the ICSD, indicating that they have yet to be experimentally prepared.

For use as a photocatalyst, the properties related to the electronic structure must be optimized. Because the band gap between the VBM and the CBM,  $E_g$ , is a measure of the electronic structure,  $E_g$  can be used to remove compounds unsuited for photocatalysis. In Figure 1a, four colors are used to distinguish the calculated  $E_g$  for the thermodynamically stable ternary compounds (the actual values are listed in Table S1 (Supporting Information)). Seven compounds have  $E_g > 2.0$  eV, which is the threshold band gap for two reasons. First, the value of  $E_g$  must be greater than the water-splitting threshold of 1.23 eV plus 0.5 eV to account for the electrochemical overpotentials. Second, experimentally reported Sn(II)-based photocatalysts such as Sn<sub>2</sub>Ta<sub>2</sub>O<sub>7</sub> and  $\beta$ -SnWO<sub>4</sub> are included in this band gap range.

After screening for the band gaps, additional calculations were performed for selected candidates to evaluate the band-edge positions relative to the vacuum level. Figure 1b compares the results to the H<sup>+</sup>/H<sub>2</sub> and O<sub>2</sub>/H<sub>2</sub>O levels, and indicates that all promising candidates are suitable photocatalysts with favorable band-edge positions, three of which are as-yet-unknown [i.e., hexagonal SnTa<sub>4</sub>O<sub>11</sub> (*P6<sub>3</sub>22*), Sn<sub>2</sub>MoO<sub>5</sub>, and SnMoO<sub>4</sub>]. It should be noted that tetragonal SnTa<sub>4</sub>O<sub>11</sub> has been reported but its structure is unknown.<sup>[26]</sup>

Herein our experimental effects focus on the SnO-MoO<sub>3</sub> system, especially SnMoO<sub>4</sub>. SnMoO<sub>4</sub> is isostructural to  $\beta$ -SnWO<sub>4</sub>, which exhibits a photocatalytic activity for the evolution of H<sub>2</sub> from an aqueous methanol solution under visible-light irradiation.<sup>[21,22]</sup> Hereafter SnMoO<sub>4</sub>, which is isostructural to  $\beta$ -SnWO<sub>4</sub>, is referred to as  $\beta$ -SnMoO<sub>4</sub>.

### 2.2. Crystal and Electronic Structures of $\beta$ -SnMoO<sub>4</sub>

After screening the compounds by DFT calculations, the crystal and electronic structures of the identified compound  $\beta$ -SnMoO<sub>4</sub> were analyzed in depth.  $\beta$ -SnWO<sub>4</sub> was also examined for comparison because experimental data are available. Figure 2a shows the theoretical crystal structure of  $\beta$ -SnMoO<sub>4</sub> after structural optimization. The calculated lattice constant of cubic  $\beta$ -SnWO<sub>4</sub> is 7.584 Å. This value is a 4% overestimate of the experimental value of 7.2989 Å,<sup>[27]</sup> which, as discussed below, is similar to the overestimated lattice constant of  $\beta$ -SnMoO<sub>4</sub>. The calculated lattice constant of  $\beta$ -SnMoO<sub>4</sub> (7.543 Å) is close to that of  $\beta$ -SnWO<sub>4</sub>, which is consistent with the fact that Mo(VI) and W(VI) ions have similar ionic radii (i.e., 55 and 56 pm, respectively, when fourfold coordinated<sup>[28]</sup>).

$\beta$ -SnMoO<sub>4</sub> is composed of MoO<sub>4</sub><sup>2-</sup> tetrahedrons and SnO<sub>3</sub><sup>4-</sup> trigonal pyramids that are corner shared. There are four distinct atomic sites: Sn (4a), Mo (4a), O1 (4a), and O2 (12b). Sn atoms are coordinated by three O2 atoms to form a trigonal pyramid. The Sn–O bond length of 2.20 Å is almost the same as that in  $\beta$ -SnWO<sub>4</sub>. Such an asymmetric coordination environment is common in Sn(II) oxides such as SnNb<sub>2</sub>O<sub>6</sub> and  $\alpha$ -SnWO<sub>4</sub>, and is a fingerprint for the formation of a lone pair. Mo is located near the center of the tetrahedron. Figure 2b compares the charge density around the Sn–O trigonal pyramid at the charge isosurface of 0.21 Å<sup>-3</sup> for  $\beta$ -SnMoO<sub>4</sub> and  $\beta$ -SnWO<sub>4</sub>. Both have a nonbonding charge density around the Sn atoms, confirming the presence of a lone pair.

The electronic band structures of  $\beta$ -SnMoO<sub>4</sub> and  $\beta$ -SnWO<sub>4</sub> are shown in Figure 2c.  $\beta$ -SnMoO<sub>4</sub> ( $\beta$ -SnWO<sub>4</sub>) shows an indirect band gap of 2.96 (3.73 eV). In both compounds, the VBM (CBM) is located at a low symmetry point along the  $\Gamma$ -X ( $M$ - $\Gamma$ ) lines. The difference between the indirect and direct gaps is only a few meV due to the very small band dispersion. The minimum direct gap is 2.96 eV for  $\beta$ -SnMoO<sub>4</sub> and 3.74 eV for  $\beta$ -SnWO<sub>4</sub>, which are almost identical with their respective indirect gaps. The total and orbital projected density of states (DOS) of  $\beta$ -SnMoO<sub>4</sub> and  $\beta$ -SnWO<sub>4</sub> in Figure 2c indicate that the VBM in both compounds is composed of Sn-5sp and O-2p orbitals. The main component of the CBM is Mo-4d or W-5d with a small contribution of Sn-5sp. The Bader charge analyses consistently indicate that the valency of Sn is 2+.

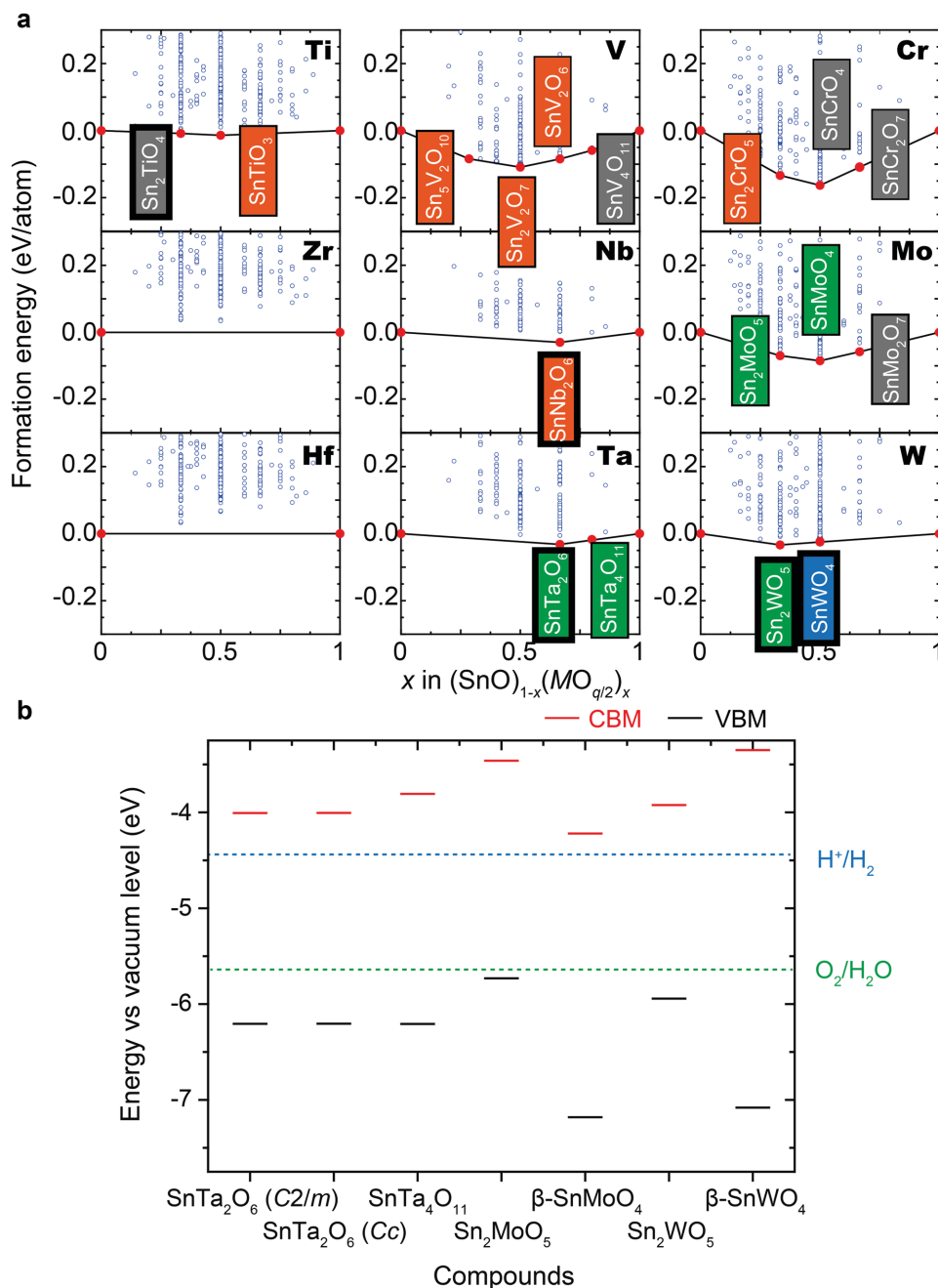


**Figure 1.** Screening results using DFT calculations. a) Blue circles show formation energy of each compound with many different crystal structures relative to the end-members (i.e., SnO and  $\text{MO}_{q/2}$ ) according to the present DFT calculations. Convex hulls for SnO- $\text{MO}_{q/2}$  pseudobinary systems are shown by black lines. Red circles correspond to compounds located either on or within 5 meV per atom above the convex hull. Thick black frame denote compounds experimentally known and registered in the ICSD. Thin black frame indicates as-yet-unknown compounds. Calculated  $E_g$  for the ternary compounds on the convex hull are categorized into four colored regions: gray:  $0 \leq E_g < 1$  eV, orange:  $1 \leq E_g < 2$  eV, green:  $2 \leq E_g < 3$  eV, and blue:  $3 \text{ eV} \leq E_g$ . When polymorphs are present, the color corresponds to the largest  $E_g$ . b) Calculated VBM and CBM against the vacuum level. Positions of the  $\text{H}^+/\text{H}_2$  and  $\text{O}_2/\text{H}_2\text{O}$  levels are from ref. [47].

Figure 2d shows the calculated optical absorption coefficients of  $\beta\text{-SnMoO}_4$  and  $\beta\text{-SnWO}_4$ . Both spectra show a steep increase near the threshold, corresponding to the electronic transition energy over the minimum direct gap. This feature should be useful for efficient light absorption, and hence, advantageous for photocatalysis.

### 2.3. Experimental Synthesis of $\beta\text{-SnMoO}_4$

The synthesis of any crystalline oxide composed of Sn(II) and Mo(VI) has yet to be reported to the best of our knowledge. Although one study claims to have synthesized  $\text{SnMoO}_4$ <sup>[29]</sup> for a humidity sensor application, the crystal structure was not

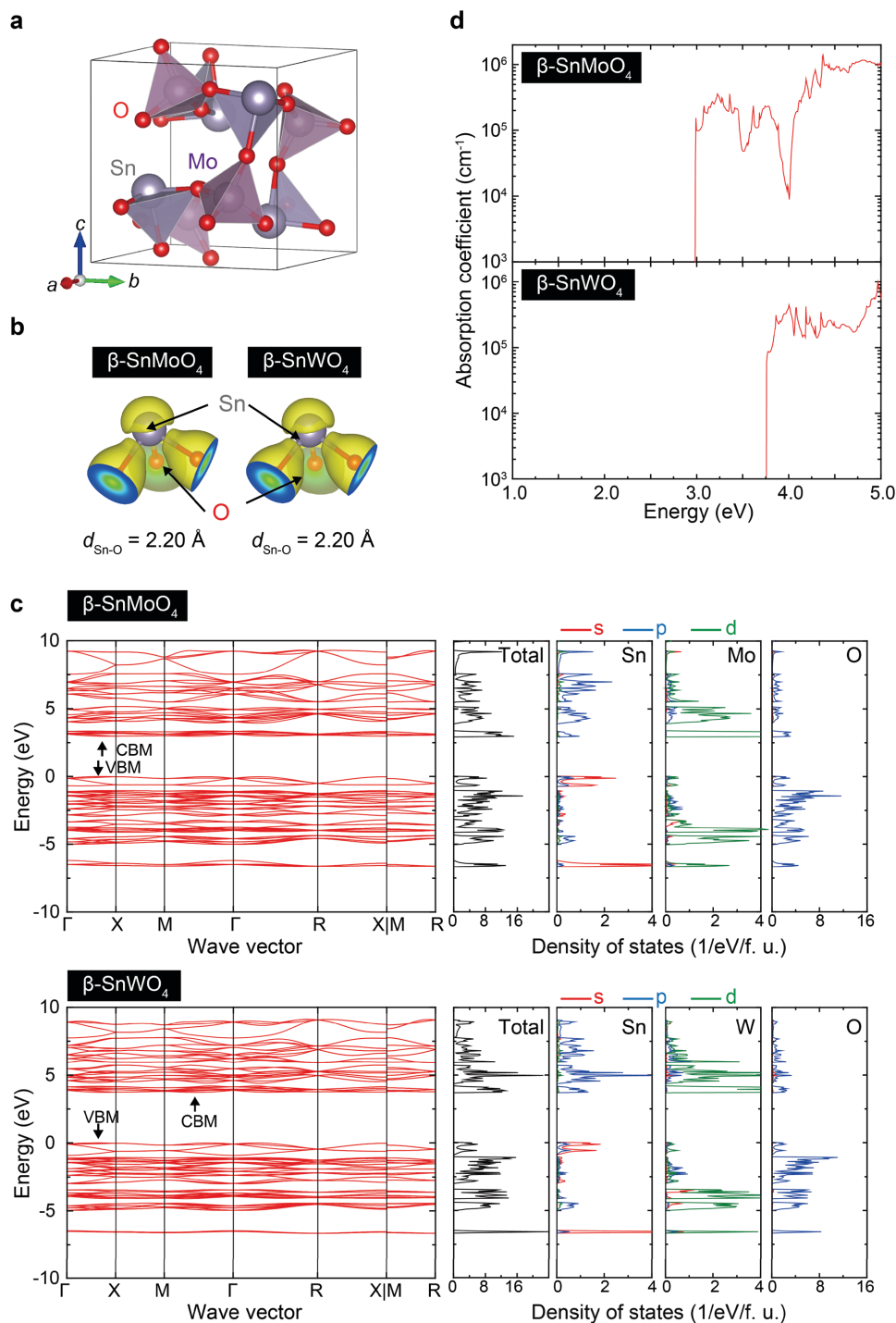


**Figure 2.** Crystal and electronic structures of  $\beta$ -SnMoO<sub>4</sub> and  $\beta$ -SnWO<sub>4</sub>. a) Theoretical crystal structures of  $\beta$ -SnMoO<sub>4</sub> after the structural optimization. b) Charge density isosurface at  $0.21 \text{ \AA}^{-3}$  around the Sn–O trigonal pyramids of both  $\beta$ -SnMoO<sub>4</sub> and  $\beta$ -SnWO<sub>4</sub>. c) Electronic band diagrams along with the total and orbital projected DOS of  $\beta$ -SnMoO<sub>4</sub> ( $M = \text{Mo}$  and  $\text{W}$ ). VBM is set to 0 eV for each  $\beta$ -SnMoO<sub>4</sub>. d) Calculated optical absorption coefficients of  $\beta$ -SnMoO<sub>4</sub> and  $\beta$ -SnWO<sub>4</sub>.

analyzed in detail, and only a simple X-ray powder diffraction (XRD) was reported. According to our experiments, a mixture of rutile-type SnO<sub>2</sub> and monoclinic MoO<sub>2</sub> (slightly distorted rutile type structure) should be formed via the synthesis conditions in ref. [29] (i.e., 998 K for 12 h in an inert atmosphere).

Indeed, the XRD profile in ref. [29] can be assigned by superposition of these two crystals as shown in Figure S2 (Supporting Information).

In the present study, we synthesized  $\beta$ -SnMoO<sub>4</sub> after many trials using various starting materials and synthesis conditions.

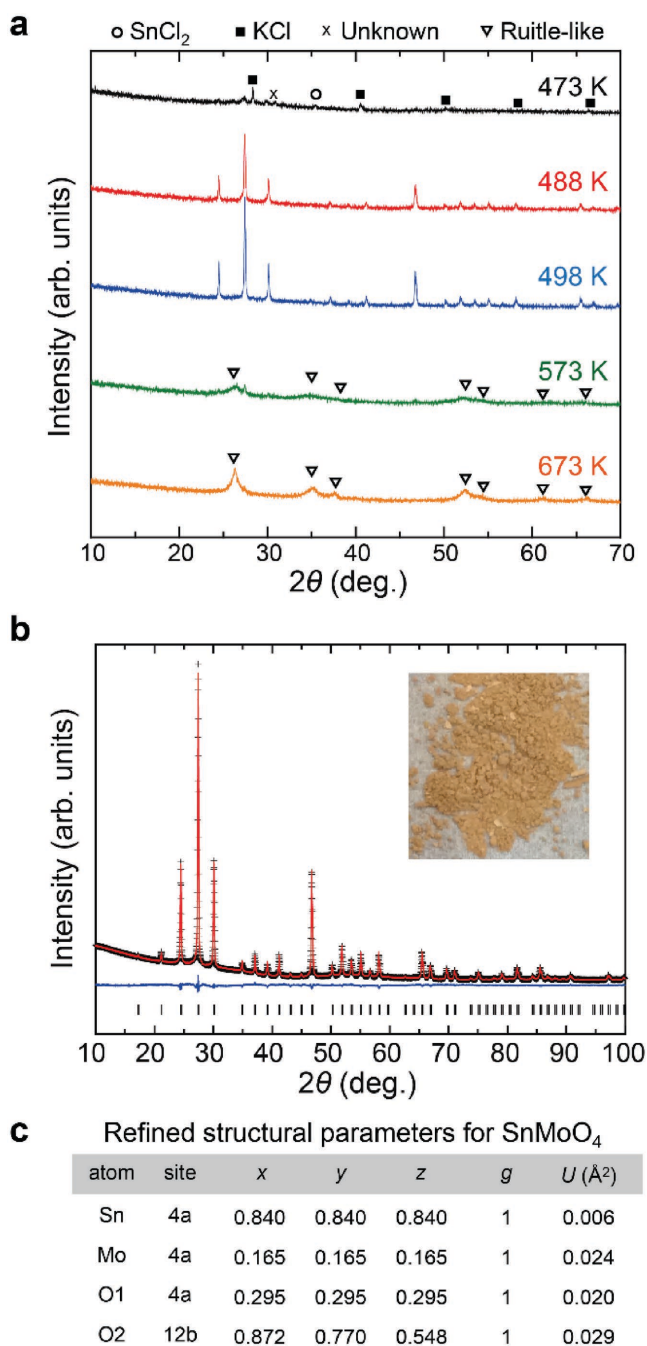


**Figure 3.** XRD profiles and crystal structure analysis of  $\beta$ -SnMoO<sub>4</sub>. a) XRD profiles of the samples obtained at a constant temperature between 473 and 673 K for 1 h under an Ar gas flow. b) XRD profile of  $\beta$ -SnMoO<sub>4</sub> prepared at 498 K (black cross) and the calculated profiles obtained by Rietveld analysis (red solid line). Solid blue line corresponds to the difference between the observed and the calculated intensities. Vertical ticks indicate the positions of the Bragg reflections. c) Refined structural parameters for  $\beta$ -SnMoO<sub>4</sub>: space group type of  $P2_13$  (No. 198), lattice constants of  $a = 7.263(7)$  Å,  $R_{wp} = 3.21\%$ ,  $R_p = 2.47\%$ , and  $S_{fit} = 3.57$  (see Figure S1 in the Supporting Information for more details).

**Figure 3a** shows the XRD profiles of the samples obtained by reacting SnCl<sub>2</sub> and K<sub>2</sub>MoO<sub>4</sub> powders at a constant temperature between 473 and 673 K for 1 h under an Ar gas flow. After cooling

to room temperature, the product was washed with distilled water and dried at 323 K. For the sample treated at 473 K, both SnCl<sub>2</sub> and KCl peaks appear despite washing. In contrast, the sample treated at 488 K results in sharp peaks, which are attributed to  $\beta$ -SnMoO<sub>4</sub>. Moreover, an exothermic reaction is detected between 473 and 488 K by differential thermal analysis, implying that a chemical reaction forms  $\beta$ -SnMoO<sub>4</sub>. For samples prepared above 573 K, the secondary phase is predominant. This secondary phase is assigned to the rutile-like SnO<sub>2</sub>-MoO<sub>2</sub> solid solution with tetragonal lattice constants of  $a = b = 4.797$  and  $c = 2.995$  Å. Increasing the temperature to 773 K results in decomposition to SnO<sub>2</sub> and MoO<sub>2</sub>, suggesting that the rutile-like SnO<sub>2</sub>-MoO<sub>2</sub> solid solution is a metastable phase.

The lattice constant and internal coordinates of  $\beta$ -SnMoO<sub>4</sub> were analyzed by the Rietveld method using the XRD profile of the sample prepared at 498 K (Figure 3b,c and Figure S3 (Supporting Information)). The cell parameter for  $\beta$ -SnMoO<sub>4</sub> (7.263 Å) is 4% smaller than the DFT lattice constant (7.543 Å). Both the cell parameter and the internal coordinate of each atom in  $\beta$ -SnMoO<sub>4</sub> are similar to those in  $\beta$ -SnWO<sub>4</sub>. The powder is bright brown (Figure 3b, inset), implying that  $\beta$ -SnMoO<sub>4</sub> has a band gap within the visible region. The Sn/Mo ratio obtained by the energy-dispersive X-ray spectrum analyzer on a scanning electron microscope (SEM-EDX) analysis is  $0.96 \pm 0.08$ .

Mössbauer experiments were performed at room temperature to examine the chemical state of Sn. Unlike the sample heated at 673 K, which is entirely in the Sn(IV) state, the sample heated at 498 K has a significant fraction of Sn in the Sn(II) state as shown in **Figure 4**. The experimental spectrum of the sample heated at 498 K can be decomposed into three components: (1) Sn(II)-1 (isomer shift  $\delta = 3.54$  mm s<sup>-1</sup>, relative to CaSnO<sub>3</sub>, quadrupole splitting  $\Delta = 1.18$  mm s<sup>-1</sup>), (2) Sn(II)-2 ( $\delta = 3.36$  mm s<sup>-1</sup>,  $\Delta = 1.75$  mm s<sup>-1</sup>), and (3) Sn(IV) ( $\delta = 0.03$  mm s<sup>-1</sup>,  $\Delta = 0.61$  mm s<sup>-1</sup>). Considering the fact that  $\beta$ -SnMoO<sub>4</sub> with a Sn(II) coordination environment is predominant in the XRD of the sample heated at 498 K, spectrum (1) is assigned to crystalline  $\beta$ -SnMoO<sub>4</sub> with a single Sn site. The large  $\Delta$  can be well explained by the trigonal pyramidal coordination environment of the Sn(II) atoms with a large electric field gradient at the Sn nucleus. The origin of spectrum (2) (areal intensity: 7%) is unclear. Spectrum (3) may be assigned to the nanocrystalline SnO<sub>2</sub>-MoO<sub>2</sub> solid solution with Sn(IV). There is evidence of a nanocrystalline SnO<sub>2</sub>-MoO<sub>2</sub> solid solution even in the XRD profile as described in Figure S1 (Supporting Information). Although the areal intensity of spectrum (1) is 28% of the total absorption, the content of  $\beta$ -SnMoO<sub>4</sub> should be larger because of the stronger temperature dependence of the recoil-free fraction of Sn(II) oxides than that of Sn(IV) oxides.<sup>[30]</sup> On the other hand, the experimental spectrum of the sample heated at 673 K can be assigned entirely to Sn(IV) oxides, which is consistent with the XRD peaks in Figure 2a that are identified as a solid solution of SnO<sub>2</sub>-MoO<sub>2</sub>.

#### 2.4. Photocatalytic Activity

The photocatalytic activity of  $\beta$ -SnMoO<sub>4</sub> powder was evaluated via the degradation of a methylene blue (MB) solution under simulated daylight irradiation. For comparison,  $\beta$ -SnWO<sub>4</sub>

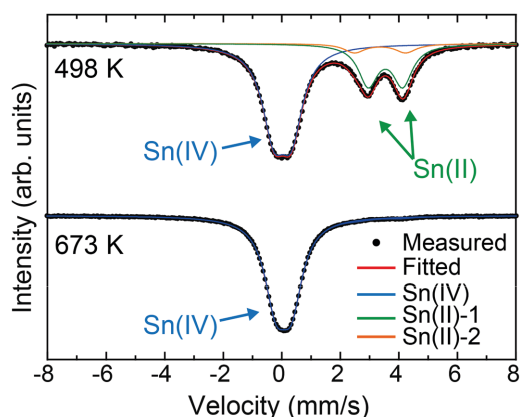


**Figure 4.**  $^{119}\text{Sn}$  Mössbauer spectra of the samples prepared at 498 and 673 K. Black dots indicate experimental spectra. Solid lines represent the fitted curves.

powder synthesized by a similar chemical route was also used for the photocatalytic activity test. **Figure 5a** shows the transmittance spectra of the MB solution with the  $\beta\text{-SnMoO}_4$  powder measured at room temperature. The peaks near 664 nm

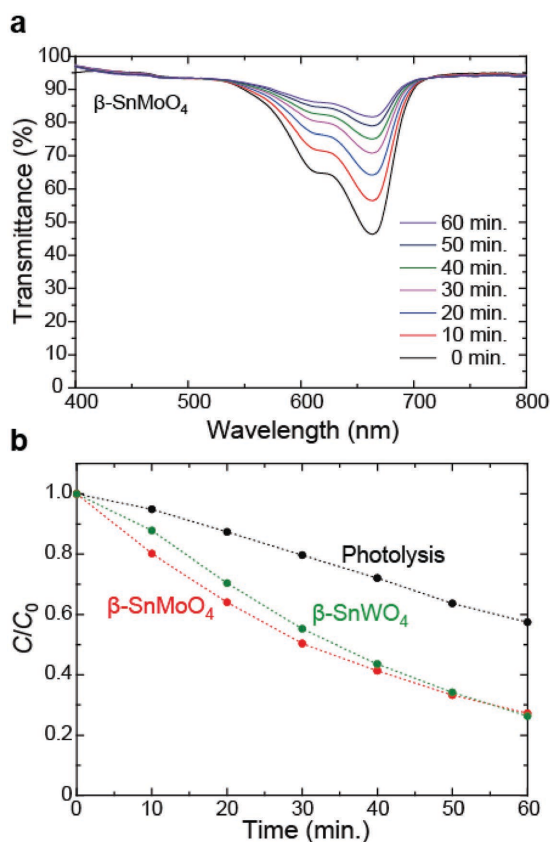


**Figure 5.** Photocatalytic activity of  $\beta\text{-SnMoO}_4$ . a) Transmittance spectra of a MB solution with  $\beta\text{-SnMoO}_4$  powder measured at room temperature. Peaks near 664 nm correspond to the absorption of MB. b) Irradiation time dependence of the relative concentration of MB solutions with and without  $\beta\text{-SnMoO}_4$  and  $\beta\text{-SnWO}_4$  powders.

correspond to the absorption of MB. The intensities of these peaks monotonically decrease upon daylight irradiation.

**Figure 5b** plots the relative concentration of the MB solution as a function of the irradiation time along with the results by MB photolysis measured under the same irradiation conditions without supplying an oxide powder. The photocatalytic activity of  $\beta\text{-SnMoO}_4$  is clear. Note that the relative concentration of the MB solution decreases only by 4% without irradiation as shown in **Figure S4** (Supporting Information). It also should be noted that the XRD profiles and the particle size of  $\beta\text{-SnMoO}_4$  and  $\beta\text{-SnWO}_4$  powders are similar to each other as shown in **Figures S5 and S6** (Supporting Information). These results imply that the photocatalytic activity of  $\beta\text{-SnMoO}_4$  powder is at least as good as that of  $\beta\text{-SnWO}_4$ , which exhibits a comparable photocatalytic activity with  $\text{BiVO}_4$ .<sup>[22]</sup> The photocatalytic activity of  $\text{BiVO}_4$  under the same experimental setup is comparatively shown in **Figure S7** (Supporting Information).

### 3. Conclusions

Through a rational search of 3483 candidate Sn(II)-based oxides, synthesis experiments, and detailed characterization, we discovered a novel oxide photocatalyst,  $\beta\text{-SnMoO}_4$ . DFT calculations were performed for the whole range of  $\text{SnO-MO}_{q/2}$  [ $M$ : Ti, Zr, and Hf ( $q = 4$ ); V, Nb, and Ta ( $q = 5$ ); Cr, Mo, and W ( $q = 6$ )] pseudobinary systems with diverse compositions and structures. Initially, the thermodynamic stability was screened, revealing that 28 compounds are located either on the convex hull or within 5 meV per atom above the convex hull (Table S1, Supporting Information). DFPT calculations of these 28 compounds indicate that only one has imaginary phonon modes at the  $\Gamma$  point, suggesting that the other 27 possess dynamic stability for the  $\Gamma$  point phonon mode. Then, the electronic structures of these thermodynamically stable ternary compounds were screened using the band gap and the band-edge positions as descriptors. Seven potential photocatalyst candidates have favorable band-edge positions.

Next we examined  $\beta\text{-SnMoO}_4$ , an unknown compound in detail. First, we developed a successful low temperature synthesis, which was confirmed by X-ray powder diffraction and Mössbauer spectroscopy. The activity of this material for the photocatalytic decomposition of the MB solution under daylight is as good as other well-studied oxide photocatalysts of  $ns^2$  cations, such as  $\beta\text{-SnWO}_4$  and  $\text{BiVO}_4$ . In addition to revealing a novel photocatalyst, this study demonstrates that a combination of high throughput screening using a large DFT database and subsequent focused synthesis experiments is a powerful tool for accelerated discovery of novel oxide photocatalysts.

### 4. Experimental Section

**DFT Calculations:** All DFT calculations were performed using the projector augmented-wave (PAW) method as implemented in the Vienna Ab initio simulation package (VASP) code.<sup>[31,32]</sup> The Perdew–Burke–Ernzerhof generalized gradient approximation (PBE-GGA)<sup>[33]</sup> was used for the screening. Table S1 (Supporting Information) summarized the calculated band gaps along with the values obtained using other approximations, including the PBEsol GGA,<sup>[34]</sup>

Tao–Perdew–Staroverov–Scuseria meta-GGA,<sup>[35]</sup> and Heyd–Scuseria–Ernzerhof 06 hybrid functional<sup>[36–38]</sup> and experimental values. The PAW data sets with radial cutoffs of 1.6, 1.5, 1.5, and 0.8 Å for Sn, Mo, W, and O, respectively, were used with a plane-wave cutoff energy of 550 eV. The Sn 5s, 5p; Mo 4p, 5s, 4d; W 6s, 5d; and O 2s, 2p states were described as valence electrons.

The crystal structures were taken from the ICSD.<sup>[23]</sup> The lattice parameters and internal coordinates were fully relaxed until the residual stresses and forces converged to less than 0.1 GPa and 0.01 eV Å<sup>-1</sup>. *k*-point sampling mesh was determined by checking the convergence of the total energy for each calculation. The optical absorption spectra were acquired via calculations of the dielectric functions within the independent particle approximation. The electron DOS and dielectric functions for β-SnMoO<sub>4</sub> (*M* = Mo and W) were calculated using a 6 × 6 × 6 *k*-point mesh. The DOS was calculated using the tetrahedron method with corrections of Blöchl et al.<sup>[39]</sup> Bader charge analyses were carried out using the Bader code<sup>[40–42]</sup> with the charge density obtained from DFT calculations. The ionization potential (IP) and electron affinity (EA), which correspond to the VBM and the CBM against the vacuum level, respectively, were calculated using the bulk-based definition according to ref. [43]. Slab–vacuum models with slab and vacuum thicknesses of ≥20 Å were obtained using the algorithm in ref. [44]. Low index nonpolar surfaces were systematically investigated, and the IP and EA values for the lowest surface energy were adopted.

**Materials Synthesis:** Polycrystalline β-SnMoO<sub>4</sub> powders were prepared by a low temperature synthesis using reagent-grade SnCl<sub>2</sub> and K<sub>2</sub>MoO<sub>4</sub> powders (Kojundo Chemical Lab. (Japan)), which were well dried at 373 K in a dry Ar gas. Stoichiometric mixtures of the starting materials were ground in an Ar atmosphere. After pelletization, the specimens were placed in an alumina crucible and heated between 473 and 673 K for 1 h under Ar gas flow. After cooling to room temperature, the product was washed with distilled water and dried at 323 K. β-SnWO<sub>4</sub> was prepared in a similar manner with a heating temperature of 483 K using K<sub>2</sub>WO<sub>4</sub> as the raw material.

**Characterization:** The crystal phases and structures were determined using an X-ray diffractometer. The lattice parameters and atomic coordinates were obtained using RIETAN FP Rietveld refinement software. The composition was measured using an SEM-EDX. Transmission<sup>119</sup>Sn Mössbauer measurements with a Ca<sup>119</sup>SnO<sub>3</sub> gamma-ray source were conducted in the constant acceleration mode at room temperature. The MB solution was photocatalytically degraded under simulated daylight using 300 W xenon lamps with a cutoff filter ( $\lambda > 350$  nm). The irradiance and irradiation angle to the water surface were set to be 400 W m<sup>-2</sup> (0.4 “SUN”) and 30°. The powder (1.9 mg of β-SnMoO<sub>4</sub> and 2.0 mg of β-SnWO<sub>4</sub>) was fixed at the bottom of the reaction cell (20 × 20 × 10 mm) with 2 mL of the MB solution (2 × 10<sup>-2</sup> mol m<sup>-3</sup>) by double-faced tape. The transmittance spectra of the sample solutions were measured every 10 min using a UV–vis spectrophotometer.

## Supporting Information

Supporting Information is available from the Wiley Online Library or from the author.

## Acknowledgements

This study was supported by the Grants-in-Aid for Scientific Research on Innovative Areas “Nano Informatics” (grant number 25106005), Scientific Research (A) (grant number 15H02286), and Scientific Research (B) (grant number 15H04125) from the Japan Society for the Promotion of Science (JSPS) and the Support Program for Starting Up Innovation Hub MI<sup>2</sup> from the Japan Science and Technology Agency. H.H. acknowledges support by a Grant-in-Aid for Young Scientists (B) (grant number 26820283) and JSPS fellowship (grant number

12J02558). Figure 2a,b was drawn using the VESTA code.<sup>[46]</sup> The Mössbauer spectroscopic measurements were performed under the Nanotechnology Platform Program by MEXT, Japan.

Received: June 29, 2016

Published online:

- [1] F. E. Osterloh, *Chem. Mater.* **2008**, *20*, 35.
- [2] Y. Wu, P. Lazic, G. Hautier, K. Persson, G. Ceder, *Energy Environ. Sci.* **2013**, *6*, 157.
- [3] W. Li, *Phys. Status Solidi RRL* **2015**, *9*, 10.
- [4] L. Mei, H. Zhao, B. Lu, *Adv. Sci.* **2015**, *2*, 1500116.
- [5] A. Togo, F. Oba, I. Tanaka, K. Tatsumi, *Phys. Rev. B* **2006**, *74*, 195128.
- [6] Y. Ogo, H. Hiramatsu, K. Nomura, H. Yanagi, T. Kamiya, M. Hirano, H. Hosono, *Appl. Phys. Lett.* **2008**, *93*, 032113.
- [7] W. Guo, L. Fu, Y. Zhang, K. Zhang, L. Y. Liang, Z. M. Liu, H. T. Cao, X. Q. Pan, *Appl. Phys. Lett.* **2010**, *96*, 042113.
- [8] A. Walsh, Y. Yan, M. Huda, M. Al-Jassim, S. Wei, *Chem. Mater.* **2009**, *21*, 547.
- [9] A. Kudo, K. Omori, H. Kato, *J. Am. Chem. Soc.* **1999**, *121*, 11459.
- [10] H. Luo, A. H. Mueller, T. M. McCleskey, A. K. Burrell, E. Bauer, Q. X. Jia, *J. Phys. Chem. C* **2008**, *112*, 6099.
- [11] K. Sayama, A. Nomura, T. Arai, T. Sugita, R. Abe, M. Yanagida, T. Oi, Y. Iwasaki, Y. Abe, H. Sugihara, *J. Phys. Chem. B* **2006**, *110*, 11352.
- [12] Q. Wang, T. Hisatomi, Q. Jia, H. Tokudome, M. Zhong, C. Wang, Z. Pan, T. Takata, M. Nakabayashi, N. Shibata, Y. Li, I. D. Sharp, A. Kudo, T. Yamada, K. Domen, *Nat. Mater.* **2016**, *15*, 611.
- [13] J. Tang, Z. Zhou, J. Ye, *Catal. Lett.* **2004**, *92*, 53.
- [14] A. Kudo, S. Hijii, *Chem. Lett.* **1999**, *28*, 1103.
- [15] H. Fu, C. Pan, W. Yao, Y. Zhu, *J. Phys. Chem. B* **2005**, *109*, 22432.
- [16] J. Tang, Z. Zou, J. Ye, *Angew. Chem., Int. Ed. Engl.* **2004**, *43*, 4463.
- [17] M. Manikandan, T. Tanabe, P. Li, S. Ueda, G. V. Ramesh, R. Kodiyath, J. Wang, T. Hara, A. Dakshinamoorthy, S. Ishihara, K. Ariga, J. Ye, N. Umezawa, H. Abe, *ACS Appl. Mater. Interfaces* **2014**, *6*, 3790.
- [18] Y. Hosogi, K. Tanabe, H. Kato, H. Kobayashi, A. Kudo, *Chem. Lett.* **2004**, *33*, 28.
- [19] K. Saito, A. Kudo, *Inorg. Chem.* **2013**, *52*, 5621.
- [20] N. Taira, T. Kakinuma, *J. Ceram. Soc. Jpn.* **2012**, *120*, 551.
- [21] I. Cho, C. H. Kwak, D. W. Kim, S. Lee, K. S. Hong, *J. Phys. Chem. C* **2009**, *113*, 10647.
- [22] J. Ungelenk, C. Feldmann, *Chem. Commun.* **2012**, *48*, 7838.
- [23] A. Belsky, M. Hellenbrandt, V. L. Karen, P. Luksch, *Acta Crystallogr.* **2002**, *58*, 364.
- [24] Materials project database, <<https://www.materialsproject.org/>> (accessed: Oct. 2015).
- [25] Aflowlib, <<http://afloplib.org/>> (accessed: Oct. 2015).
- [26] D. Bodiöt, *Rev. Chim. Miner.* **1968**, *5*, 569.
- [27] W. Jeitschko, A. W. Sleight, *Acta Crystallogr. B* **1972**, *28*, 3174.
- [28] R. D. Shannon, *Acta Crystallogr. A* **1976**, *32*, 751.
- [29] A. M. E. S. Raj, C. Mallika, O. M. Sreedharan, K. S. Nagaraja, *Mater. Res. Bull.* **2001**, *36*, 837.
- [30] G. S. Collins, T. Kachnowski, N. Benczer-Koller, M. Pasternak, *Phys. Rev. B* **1979**, *19*, 1369.
- [31] G. Kresse, J. Furthmüller, *Phys. Rev. B* **1996**, *54*, 11169.
- [32] G. Kresse, D. Joubert, *Phys. Rev. B* **1999**, *59*, 1758.
- [33] J. P. Perdew, K. Burke, M. Ernzerhof, *Phys. Rev. Lett.* **1996**, *77*, 3865.
- [34] J. P. Perdew, A. Ruzsinszky, G. I. Csonka, O. A. Vydrov, G. E. Scuseria, L. A. Constantin, X. Zhou, K. Burke, *Phys. Rev. Lett.* **2008**, *100*, 136406.
- [35] J. Sun, M. Marsman, G. I. Csonka, A. Ruzsinszky, P. Hao, Y. Kim, G. Kresse, J. P. Perdew, *Phys. Rev. B* **2011**, *84*, 035117.

- [36] J. Heyd, G. E. Scuseria, M. Ernzerhof, *J. Chem. Phys.* **2003**, *118*, 8207.
- [37] J. Heyd, G. E. Scuseria, M. Ernzerhof, *J. Chem. Phys.* **2006**, *124*, 219906.
- [38] A. V. Krugau, O. A. Vydrov, A. F. Izmaylov, G. E. Scuseria, *J. Chem. Phys.* **2006**, *125*, 224106.
- [39] P. E. Blöchl, O. Jepsen, O. K. Andersen, *Phys. Rev. B* **1994**, *49*, 16223.
- [40] G. Henkelman, A. Arnaldsson, H. Jónsson, *Comput. Mater. Sci.* **2006**, *36*, 354.
- [41] E. Sanville, S. D. Kenny, R. Smith, G. Henkelman, *J. Comput. Chem.* **2007**, *28*, 899.
- [42] W. Tang, E. Sanville, G. Henkelman, *J. Phys.: Condens. Matter* **2009**, *21*, 084204.
- [43] Y. Hinuma, F. Oba, Y. Kumagai, I. Tanaka, *Phys. Rev. B* **2012**, *86*, 245433.
- [44] Y. Hinuma, Y. Kumagai, F. Oba, I. Tanaka, *Computational Mater. Sci.* **2016**, *113*, 221.
- [45] F. Izumi, K. Momma, *Solid State Phenom.* **2007**, *130*, 15.
- [46] K. Momma, F. Izumi, *J. Appl. Crystallogr.* **2011**, *44*, 1272.
- [47] S. Trasatti, *Pure Appl. Chem.* **1986**, *58*, 955.
-